GEOPHYSICAL RESEARCH LETTERS, VOL. ???, XXXX, DOI:10.1029/,

Rates of thermohaline recovery from freshwater pulses in Modern, Last Glacial Maximum and Greenhouse Warming Climates

C. M. Bitz[1], J. C. H. Chiang[2], W. Cheng[3], and J. J. Barsugli[4]

Recovery rates of the thermohaline circulation after a freshwater pulse in the North Atlantic vary considerably depending on the background climate, as demonstrated in the Community Climate System Model. The recovery is slowest in a Last Glacial Maximum (LGM) climate, fastest in a modern climate, and intermediate between the two in a greenhouse warming ($4XCO_2$) climate. Previously proposed mechanisms to explain thermohaline circulation stability involving altered horizontal freshwater transport in the North Atlantic are consistent with relative recovery rates in the modern and $4XCO_2$ climates, but fail to explain the slow LGM recovery. Instead, sea ice expansion inhibits deep-water formation after freshening in the LGM climate by reducing heat loss to the atmosphere and providing additional surface freshwater. In addition, anomalous vertical freshwater transport across ∼1km depth after freshening is most effective at weakening the stratification in the modern case but is negligible in the LGM case.

1. Introduction

Shutdown of the thermohaline circulation (THC) in a modern climate from enhanced freshwater input of roughly ∼10 Sv-yr (1 Sv = $10^6 m^3 s^{-1}$) to the North Atlantic is usually only temporary in climate models: Once the freshwater input returns to normal, the circulation recovers in a few decades to a century at most [*Stouffer et al.*, 2006]. These models agree roughly with the duration of climate change that followed meltwater pulses approximately 8200 year ago, which resulted in the largest global cooling in the Holocene [*Ellison et al.*, 2006]. However, meltwater pulses of a similar magnitude during the most recent glacial are hypothesized to have caused the THC to remain collapsed or greatly reduced for much longer durations [see e.g., *Clark et al.*, 2002]. It remains to be seen how anthropogenic climate change and the anticipated increase in precipitation and runoff in the northern North Atlantic will influence the THC response to freshwater pulses, say from Greenland.

Here we investigate the influence of the climate state on THC recovery following a freshwater addition to the North Atlantic using the Community Climate System Model Version 3 (CCSM3). We add the same freshwater anomaly to modern, greenhouse warming, and glacial climates to investigate the mechanisms of THC recovery in a spectrum of background climates.

2. Model

We impose freshwater perturbations to three nearly equilibrated background climate cases: a 1,000 yr integration with "modern" (i.e., 1990s) conditions [*Collins et al.*, 2006], a 440 yr Last Glacial Maximum LGM (with ice-sheet topography, ocean bathymetry, orbital configuration, and greenhouse gases prescribed for ∼21 ka) integration [*Otto-Bliesner et al.*, 2006], and a $4XCO_2$ stabilization integration [*Bryan et al.*, 2006] where CO_2 is initially increased at the rate of 1% per year from present-day to four times present-day levels and then held fixed for 300 yr. These particular background climates, or "controls", were chosen to sample a wide range of initial THC strengths and structures and surface heat and freshwater fluxes.

We branched freshwater pulse experiments from each control by instantaneously freshening the upper 970m of the North Atlantic and Arctic Oceans from 55-90°N, 90°W-20°E by an average of 2psu (higher at the top and tapering with depth). This is equivalent to adding 16 Sv-yr of freshwater. Our method is similar to *Vellinga et al.* [2002] and contrasts with that used in the intercomparison study described by *Stouffer et al.* [2006], where freshwater is added over 100 yr to the surface. The latter distributes the freshening over time, while the former distributes it in depth. Neither is obviously more realistic, but instantaneous freshening is more computationally efficient for studying THC recovery. We conducted seven freshened runs for a minimum of 20 yr each (three modern, three LGM, and one $4XCO_2$). One member from each climate is longer (75 yr for modern and $4XCO_2$ and 135 yr for LGM) to capture the decade to century time-scale recovery. Ad-

[1]Dept. of Atmospheric Sciences, University of Washington
[2]Dept. of Geography and Center for Atmospheric Sciences, University of California, Berkeley
[3]JISAO/School of Oceanography, University of Washington
[4]CIRES, University of Colorado

0094-8276/07/$5.00

ditional information about the model and experiments is given in the auxiliary materials.

3. Results

Freshening in the North Atlantic causes the THC to immediately collapse with a cessation of North Atlantic Deep Water (NADW) formation in all seven runs as shown in Fig. 1. In no case is the collapse permanent, but the recovery rates are strikingly different depending on the background climate state. The range of recovery rates within each three-member ensemble is clearly much smaller. After a complete collapse and even reversal in year one, every run exhibits an initial rapid increase to 2–5 Sv by year 4, and then weakens again in years 5–10 (see Fig 1). After year 10 the modern THC rapidly recovers at a rate of $\sim$0.2 Sv yr^{-1}. In contrast, the LGM THC recovery rate is about 10 times slower, or $\sim$0.02 Sv yr^{-1}. The 4XCO$_2$ recover rate is $\sim$0.07 Sv yr^{-1} — intermediate to the other two. According to Fig 1, the THC recovery takes about $\sim$40 yr in the modern case and about $\sim$70 yr in the 4XCO$_2$ case, while the LGM case appears as though it could take several centuries. This dependence of the THC recovery rate on the climate state is the main finding of this study. In the rest of this section we evaluate several possible explanations.

One might expect the recovery rate to depend on the degree to which the THC is controlled by thermal versus haline forcing in the different climates. Using a simple box model, *Rahmstorf* [1996] argued that the direction of freshwater transport by the meridional overturning circulation, W_{THC}, at 33°S indicates whether the THC at equilibrium is exclusively thermally driven (southward W_{THC}) or both thermally and haline driven (northward W_{THC}). W_{THC} is computed from

$$W_{\mathrm{THC}} = -\frac{1}{S_o}\int \bar{v}(\bar{S} - S_o)dz, \qquad (1)$$

where $\bar{v}$ is the zonally integrated northward velocity, $\bar{S}$ is the zonal mean salinity, and S_o is the reference salinity, taken here as the global mean salinity. *Rahmstorf* [1996] explained that a southward W_{THC} salinifies the Atlantic, so at equilibrium the sum of all other Atlantic freshwater contributers must brake the THC, rather than drive it. In this case, a THC shutdown eliminates a salinity source to the Atlantic, which sustains the shutdown by providing a positive feedback. If the shutdown is only temporary, then positive feedbacks slow the recovery. A parallel argument suggests a northward W_{THC} yields a negative feedback, which aids recovery. *de Vries and Weber* [2005] found this reasoning worked well to describe a series of experiments in an intermediate complexity model where they varied W_{THC} at 33°S by applying surface freshwater flux adjustments.

Table 1. THC recovery rates and Atlantic northward freshwater fluxes

Background Climate	Recovery Rate	Control W_{THC} 33°S	Perturbed* ΔW_{gyre} 33°N
LGM	0.02 Sv yr^{-1}	0.26 Sv	-0.47 Sv
Modern	0.2 Sv yr^{-1}	0.03 Sv	-0.33 Sv
4XCO$_2$	0.07 Sv yr^{-1}	-0.02 Sv	-0.30 Sv

* 2nd decade after freshening

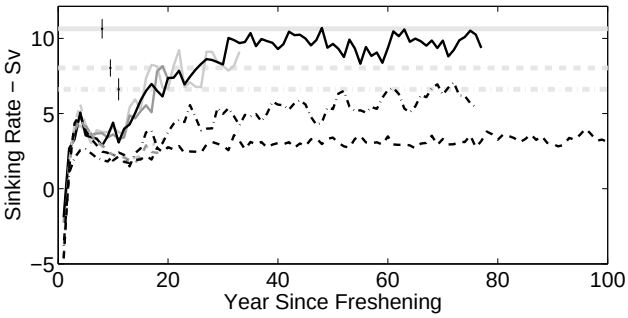

Figure 1. Annual mean thermohaline circulation index (solid lines = modern, dashed = LGM, dot-dash = 4XCO$_2$). The light gray lines show the mean index for the corresponding control runs with error bar indicating plus/minus one standard deviation. The index is the sinking flux across 1022 m depth from 60-65°N, which emphasizes changes in NADW formation rate, as suggested by *Gent* [2001]. Positive (negative) values indicate sinking (upwelling). An index of the THC using the maximum of the Atlantic meridional overturning streamfunction yields the same general conclusions (see auxiliary materials).

In our runs, only the 4XCO$_2$ control has a southward W_{THC} (see Table 1). Because freshening the 4XCO$_2$ climate does not cause a permanent THC collapsed, other negative feedbacks must be operative. However, if we assume these other feedbacks are about the same strength for all three climate states, so that W_{THC} determines the relative rate of recovery, then the LGM case should recover fastest, with the modern case next, and the 4XCO$_2$ case last. Because the LGM case is actually the slowest to recover, we can conclude that other feedbacks must control the LGM recovery.

Vellinga et al. [2002] argued that the THC recovery after freshening was controlled by anomalous salt advection from the North Atlantic subtropical gyre. The salinity flux by the gyre is typically expressed in terms of a freshwater flux:

$$W_{\mathrm{gyre}} = -\frac{1}{S_o}\int \overline{v'S'}dz, \qquad (2)$$

where S' and v' are deviations from the zonal means and the overbar indicates a zonal integral. After freshening, *Vellinga et al.* [2002] found W_{gyre} at 25°N decreased

owing to a southward shift of the Atlantic ITCZ. The nature of the ITCZ shift after freshening depends on the mean climate state (Cheng et al, submitted). The ITCZ shift serves as a negative feedback on the THC, such that a larger decrease in W_{gyre} in the subtropical North Atlantic promotes a faster recovery. However, W_{gyre} at 33°N in the Atlantic decreases more after freshening the LGM climate than the modern or $4XCO_2$ climates (see Table 1), and thus cannot explain the slow LGM recovery.

The role of surface buoyancy forcing on NADW formation is another potential factor influencing the THC recovery rate. The presence of the sea ice strongly alters the surface buoyancy forcing in the subpolar seas, so we compare the sea ice cover in relation to the surface density in the freshened region for the three control climate states. Figure 2a shows that in the LGM control sea ice of 30–80% concentration covers the densist outcroppings, where NADW forms (also roughly where the mixed layer reaches its maximum depth, see auxiliary material.), suggesting a larger haline influence on the THC in the LGM climate. This is in agreement with paleoclimate evidence of brine rejection contributing to glacial NADW formation [*Vidal et al.*, 1998]. In contrast, NADW formation occurs south of the sea ice edge in the modern and 4xCO2 controls (Fig. 2b and c). Freshening causes the sea ice cover to expand in all cases, but little sea ice reaches the NADW formation sites in the modern and $4XCO_2$ climates. This disparity in sea ice cover among the climates changes the nature of feedbacks involving the surface fluxes that drive the THC recovery through deep-water formation.

To quantify the effect of surface buoyancy flux forcing on watermass formation [see *Speer and Tziperman*, 1992], we first compute components of the surface density flux, $-\rho\alpha F_T$ and $\rho\beta F_S$, where ρ is the seawater density, α and β are seawater thermal and haline contraction coefficients, and F_T and F_S are surface heat and freshwater fluxes. The density flux components are integrated over density outcroppings in the Atlantic north of 55°N, south of the Arctic Ocean, and west of the Barents Sea (henceforth called the "North Atlantic freshened region") to arrive at a watermass transformation function $\tau_{S,T}$. Finally we take the derivative, $\partial\tau_{S,T}/\partial\rho$, to give the surface watermass formation rate (WFR) as a function of ρ (with units $\text{Sv}(\text{kg/m}^3)^{-1}$) for each component. As such, the only other sources of buoyancy forcing to a given density range are from diapycnal mixing and boundary flow. If we imagine placing a bottom "boundary" on isopycnals at 1022 m depth

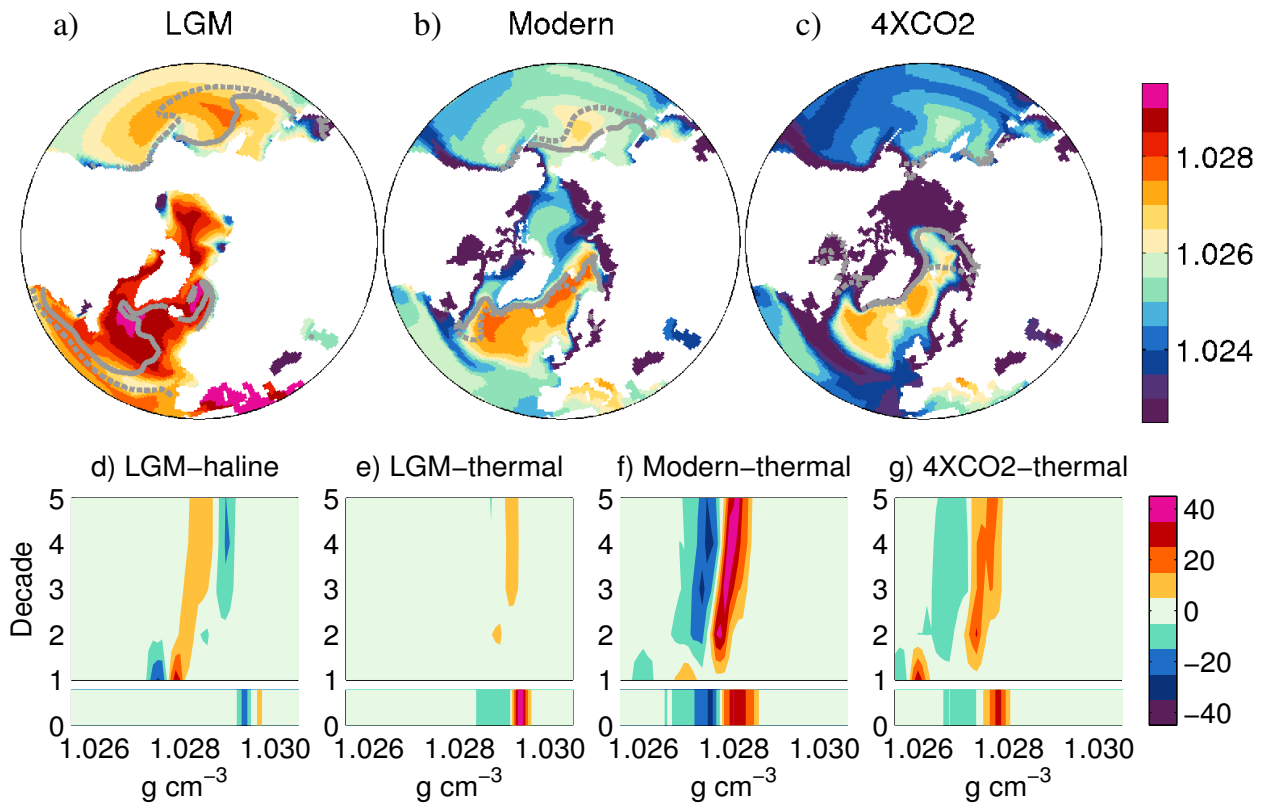

Figure 2. (a-c) Annual mean surface density in the controls in g cm^{-3} with the 15% sea ice concentration contour in the controls (solid lines) and in the second decade after freshening (dashed lines). (d-g) Watermass formation rate in Sv $(\text{kg/m}^3)^{-1}$ for the North Atlantic freshened region in the control (decade 0) and after freshening (decades 1–5). Haline components for the modern and $4XCO_2$ are negligible and not shown.

in the sinking region, then the flow across this boundary (i.e., our index of the THC in Fig. 1) is equal to the WFR from surface fluxes summed over all isopycnals that cross this boundary plus the diapycnal mixing into these isopycnals between the surface and 1 km depth.

Figure 2d-g shows WFR for the North Atlantic freshened region for all non-negligible thermal and haline components in our runs. The rate that surface fluxes further densify the heaviest outcroppings (creating NADW) is indicated by the magnitude of the rightmost maxima. The thermal component dominates NADW formation in all three controls and also after freshening in the modern and $4XCO_2$ climates. *Only the LGM case develops a substantial haline component after freshening.* Freshening shifts the whole pattern to the left, as outcroppings are made lighter. Then as the freshwater anomaly erodes, the pattern travel rightward, back towards its position in the control. (However, the physical location of the heaviest outcroppings and deepest mixed layer sites are not altered by freshening, see auxiliary material.) In the modern case, surface heat fluxes create dense watermasses at an even higher rate than in the control within two decades after freshening, despite the shift in density (Fig. 2f). In the $4XCO_2$ case, surface heat fluxes create dense watermasses after freshening at about 70% of the control rate (Fig. 2g). In contrast, the LGM case has greatly reduced dense water formation after freshening (Fig. 2d and e) owing to expanded sea ice cover over deep-water outcroppings. Sea ice in the LGM climate is transported further south and east, where it reduces heat loss and provides a new source of surface freshwater after freshening that destroys outcroppings with $\rho \sim 1.029 \mathrm{gcm}^{-3}$. There is some compensating increased brine rejection along with reduced precipitation (discussed in the auxiliary material) over less dense waters, with $\rho \sim 1.028 \mathrm{gcm}^{-3}$ (Fig. 2d). Such a mechanism involving sea ice was proposed by *Stocker et al.* [2001]. The reversal of the effective salt flux over the densest water outcroppings, counteracting the thermal forcing after freshening, is the signature of a fundamental difference between the LGM climate and the modern and $4XCO_2$ climates.

The WFR we computed only depends on surface buoyancy forcing, yet the THC strength and structure also depends on the internal ocean stratification. Among our control simulations, the modern ocean is the least stable below about 900 m (see Fig. 3a), consistent with its higher sinking rate in Fig. 1 and the greater sinking depths reached by its NADW compared to the other controls [*Otto-Bliesner et al.*, 2006; *Bryan et al.*, 2006]. Comparably greater stratification in the LGM control is due mainly to salinity, in broad agreement with paleo evidence [*Labeyrie*, 1992], while in the $4XCO_2$ control it is due mainly to temperature (not shown). Weaker stratification below the freshened layer in the modern case allows faster vertical dissipation of the freshwater anomaly, as can be seen in the potential density anomaly five decades after freshening in Fig. 3b. The downward anomalous freshwater flux at 1022 m and 1501 m depths is largest in the modern case and smallest in the LGM case (Fig.3c). Anomalous downward freshwater transport erodes the high stratification that was imposed by freshening and assists in the THC recovery. This salinity homogenization after freshening is most effective in the modern case and least effective in the LGM case. After five decades, LGM and $4XCO_2$ anomaly profiles below 1km depth are clearly more stabilizing than the modern anomaly profile (Fig. 3b). The strong implication is that the originally more stable density profiles below the surface layer in the LGM and $4XCO_2$ controls inhibit dissipation of the salinity anomaly by transport [as noted by *Tziperman et al.*, 1994] and by convection [as noted by *Lenderink and Haarsma*, 1993].

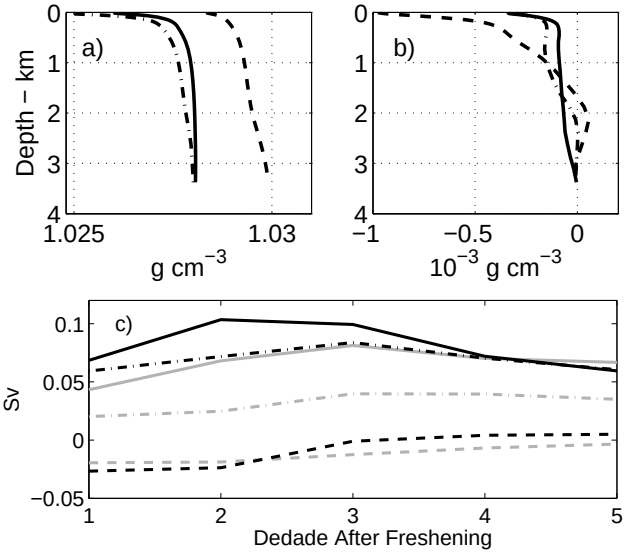

Figure 3. Density profiles in the (a) controls and (b) anomalies five decade after freshening and anomalous vertical freshwater flux (c) through 1022m (black) and 1501m (grey). All quantities are averaged over the North Atlantic freshened region. The reference salinity used to compute the freshwater flux in (c) is the average salinity above 3.125 km depth in the region. (Solid line = modern, dashed = LGM, dot-dash = $4XCO_2$.)

We also examined the horizontal freshwater transport into and out of the northern North Atlantic (integrated over the entire water column in the freshened region), as well as the surface freshwater flux. The total rate at which the freshwater anomaly dissipates from the water column depends little on the climate state (see auxiliary material). *Hu et al.* [2007] found the THC recovers more rapidly when the Bering Strait is open (compared to closed) in a modern climate in CCSM ver-

sion 2 after adding freshwater at the rate of 1 Sv for 100 yr. Because their freshwater was added at the surface, the anomaly remains more surface bound. In turn, a sizeable fraction escapes through the 50 m deep Bering Strait when it is open. In contrast, when we prescribe less than 1/6 of the total freshwater anomaly that was used by Hu et al and we distribute it over the upper 970 m, we find only about 1/16 of this anomaly escapes through Bering Strait in our modern case. Thus Freshwater need not escape through Bering Strait in CCSM3 for the THC recovery to be rapid. It is also noteworthy that the THC recovery in our $4XCO_2$ freshened case is much less rapid than in the modern case, despite Bering Strait being open in both.

4. Summary and Conclusions

We have shown that the recovery rate from a temporary collapse of the thermohaline circulation after freshening in the north Atlantic depends on the background climate state in CCSM3. Clearly, the recovery rate from a given freshwater pulse in models with present day conditions is not a good indication of the recovery rate from a pulse of the same magnitude and location in a $4XCO_2$ or glacial climate.

We analyzed recovery mechanism that are influenced by horizontal freshwater transport by the mean meridional circulation at 33°S and by the subtropical gyre in the North Atlantic. If these were the dominant feedback mechanism in our model, then the LGM case would have the fastest recovery followed by the modern, with the $4XCO_2$ case being the slowest.

A mechanism that slows the recovery in the LGM case is the expansion of sea ice in the NADW formation regions. NADW formation via surface fluxes in the LGM freshened case alone is inhibited by sea ice expansion, which effectively reduces surface heat loss and supplies meltwater over deep-water outcroppings. In contrast, surface heat loss drives NADW formation in the modern and $4XCO_2$ climates within two decades after freshening. Sea ice in poised to play a greater role in the LGM climate because *NADW production sites are partially covered with sea ice even before freshening.*

After freshening the combination of the anomalous horizontal freshwater transport and surface freshwater flux in the North Atlantic freshened region are roughly the same in all three cases. Therefore the dissipation rate of the total freshwater anomaly through the surface and lateral boundaries cannot explain the differing recover rates. Instead, we find that the anomalous downward freshwater transport across ∼1km depth is effective at weakening the stratification in the modern case after freshening, while the same flux is smaller in the $4XCO_2$ and nearly zero in the LGM case.

Acknowledgments. We gratefully acknowledge support from the National Science Foundation through grant ATM-0502204. Computational facilities were provided by the National Center for Atmospheric Research (NCAR).

References

Bryan, F., G. Danabasoglu, N. Nakashiki, Y. Yoshida, D.-H. Kim, J. Tsutsui, and S. Doney, Response of the North Atlantic thermohaline circulation and venticlation to increasing carbon dioxide in CCSM3, *J. Climate*, *19*, 2382–2397, 2006.

Clark, P. U., N. G. Pisias, T. F. Stocker, and A. J. Weaver, The role of the thermohaline circulation in abrupt climate change, *Nature*, *415*, 863–869, 2002.

Collins, W. D., et al., The Community Climate System Model, Version 3, *J. Climate*, *19*, 2122–2143, 2006.

de Vries, P., and S. L. Weber, The atlantic freshwater budget as a diagnostic for the existence of a stable shut down of the meridional overturning circulation, *Geophys. Res. Lett.*, *32*, doi:10.1029/2004GL021450, 2005.

Ellison, C. R. W., M. R. Chapman, and I. R. Hall, Surface and deep ocean interactions during the cold climate event 8200 years ago, *Science*, *312*, 1929–1932, 2006.

Gent, P. R., Will the North Atlantic Ocean thermohaline circulation weaken during the 21st century?, *Geophys. Res. Lett.*, *28*, 1023–1028, 2001.

Hu, A., G. A. Meehl, and W. Han, Role of the Bering Stait in the thermohaline circulation and abrupt climate change, *Geophys. Res. Lett.*, *in press*, 2007.

Labeyrie, L., Changes in vertical structure of the North Atlantic Ocean between glacial and modern times, *Quat. Sci. Rev*, *11*, 401–413, 1992.

Lenderink, G., and R. J. Haarsma, Variability and multiple equilibria of the thermohline circulation associated with deep-water formation, *J. Phys. Oceanogr.*, *24*, 1480–1493, 1993.

Otto-Bliesner, B. L., E. C. Brady, G. Clauzet, R. Tomas, S. Levis, and Z. Kothavala, Last glacial maximum and holocene climate in CCSM3, *J. Climate*, *19*, 2526–2544, 2006.

Rahmstorf, S., On the freshwater forcing and transport of the Atlantic thermohaline circulation, *Clim. Dyn.*, *12*, 799–811, 1996.

Speer, K., and E. Tziperman, Rates of watermass formation in the North Atlantic Ocean, *J. Phys. Oceanogr.*, *22*, 93–110, 1992.

Stocker, T. F., R. Knutti, and G.-K. Plattner, The future of the thermohaline circulatio — a perspective, in *The Ocean and Rapid Climate Changes: Past, Present, and Future*, pp. 277–293. Geophysical Monograph 126, American Geophysical Union, 2001.

Stouffer, R. J., et al., Investigating the causes of the response of the thermohaline circulation to past and future climate changes, *J. Climate*, *19*, 1365–1387, 2006.

Tziperman, E., J. R. Toggweiler, Y. Feliks, and K. Bryan, Instability of the thermohaline circulation with respect to mixed boundary conditions: Is it really a problem for realistic models, *J. Phys. Oceanogr.*, *24*, 217–232, 1994.

Vellinga, M., R. Wood, and J. M. Gregory, Processes governing the recovery of a perturbed thermohaline circulation in HadCM3, *J. Climate*, *16*, 2002.

Vidal, L., L. Labeyrie, and T. C. E. van Weering, Benthic $\delta^{18}O$ records in the North Atlantic over the last glacial period, *Paleoceanography*, *13*, 245–251, 1998.

C. M. Bitz, Dept. of Atmospheric Sciences, MS 351640, University of Washington, Seattle, WA 98195-1640. (bitz@atmos.washington.edu)

Auxiliary Materials - online only

The Community Climate System Model (CCSM3) used in this study has an atmosphere component with approximately 2.8° horizontal resolution (T42 spectral truncation) and 26 vertical levels. The ocean and sea ice have zonal resolution of 1.125° and the meridional resolution of 0.54°, except in the subtropics and tropics where the meridional resolution is finer. CCSM3 is well documented and may be downloaded freely from http://www.ccsm.ucar.edu. Present-day forcing is fixed at 1990 levels for anthropogenic greenhouse gases (CO_2 = 355ppm, CH_4 = 1714ppb, and N_2O= 311ppb), ozone, and aerosols. and has LGM greenhouse gas concentrations (CO_2 = 185ppm, CH_4 = 350ppb, and N_2O= 200ppb) estimated from icecores. Ozone and aerosol forcing are set to pre-industrial estimates for the LGM and to 1990 estimates for the modern and $4XCO_2$ simulations.

Individual ensemble members were branched from different times in the controls to sample a range of initial conditions. Results for the first 20 yr are averaged over the three ensemble members for the modern and LGM freshened cases.

Figure A shows a timeseries of the maximum of the meridional overturning streamfunction in the North Atlantic, which is an often-used measure of the THC strength and is an alternative to the index used in the main text. The maximum overturning occurs at about 35°N at a depth of 850m in the modern control in CCSM3. The average value of the maximum overturning for the three controls is approximately double the sinking flux across 1022 m depth from 60-65°N, the measure of THC strength used in the main text. The transient behavior of the THC after freshening appears qualitatively similar in the two measures. The recovery rate in the modern climate is fastest, at least in the first 40 years after freshening, and the recovery rate in the $4XCO_2$ modern climate is intermediate between the modern and LGM rates. There are subtle differences in the details of the recovery as measured by the two THC indices. Such differences in the various measures of the THC strength during transient changes have been described previously and are expected [*Gent*, 2004]. In fact, these subtle differences are evidence that more than one measure of the THC should be considered when analyzing North Atlantic climate. However, none of the results and conclusions in the main text are influenced substantially by the choice of THC index.

Figure 2 shows the annual mean mixed layer depths in the controls and their anomalies after freshening. This figure shows that the locations with annual mean mixed layer depths over 200 m roughly coincide with the locations of the heaviest density outcroppings at the surface in Fig 2. The mixed layer becomes shallower in most places after freshening, but the location of the maxima do not shift in any remarkable way. The maximum mixed layer depths remain underneath the sea ice before and after freshening in the LGM climate and south of the sea ice edge before and after freshening in the modern and $4XCO_2$ climates.

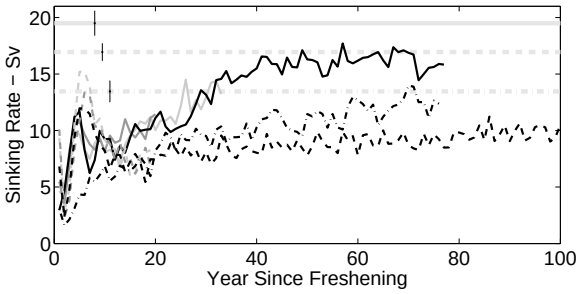

Figure A. Alternative index of the annual mean thermohaline circulation shown in Fig 1. Here the index is the maximum of the Atlantic meridional overturning streamfunction north of 20°N and below 418m depth. (Solid line = modern, dashed = LGM, dot-dash = $4XCO_2$).

Figure 3a shows horizontal (depth integrated) freshwater fluxes into the northern North Atlantic freshened region across ∼55°N and at the interface of the Arctic and Barents Seas and the freshwater flux into the surface of the region. These individual components of the freshwater budget depend on the climate state. However, the total freshwater dissipation rate (Fig. 3b) is roughly the same for all three climates, so the total freshwater dissipation does not provide an explanation for the large differences in the THC recovery rates. Because the horizontal transports are integrated vertically, the important influence of the vertical freshwater flux (see Fig 3 and the main text) is not apparent. Nonetheless the routes of horizontal freshwater dissipation are worth mentioning. In the first decade after freshening, Fig. 3a shows that there is anomalous freshwater export to the north and south in all cases. The anomalous southward export at ∼55°N, which is comparable in the first decade in all three cases, is due to the export of the freshened, near-surface waters by the Labrador Current. The anomalous northward export into the Arctic and Barents Sea is at least three times larger in the first decade in the modern and $4XCO_2$ cases, which have Bering Strait open, than in the LGM case. Instead, the LGM has a considerable reduction in precipitation on average over the freshened region, which is unseen in the modern and $4XCO_2$ cases. The reduction in precipitation in the LGM climate occurs over a large area, while there is increase in the convergence of sea ice with even greater magnitude but localized over deep-water outcroppings in the LGM (see Fig 2d). In all three cases the total freshwater dissipation rate is about an order of magnitude larger in the first decade after freshening that in subsequent decades.

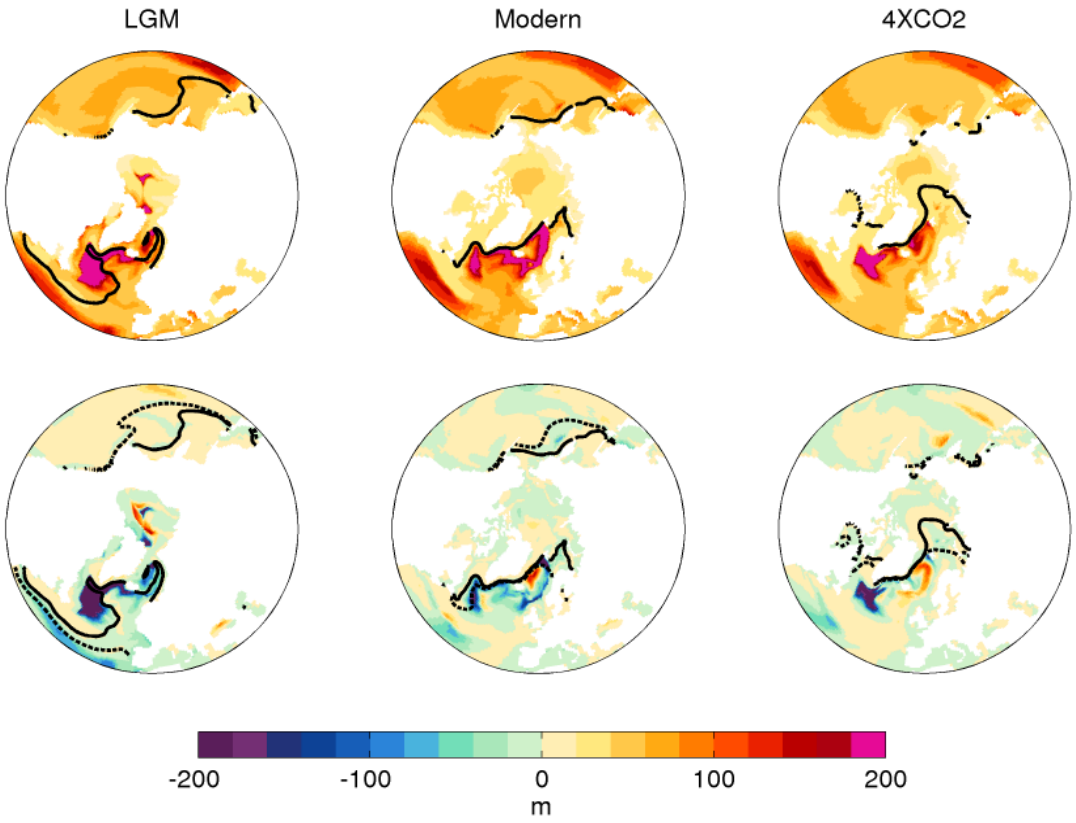

Figure 2. Annual mean mixed layer depths in the controls (upper panels) and the anomalies two decades after freshening (lower panels) with the 15% sea ice concentration contour in the controls (solid black line) and two decades after freshening (dashed, lower panels only).

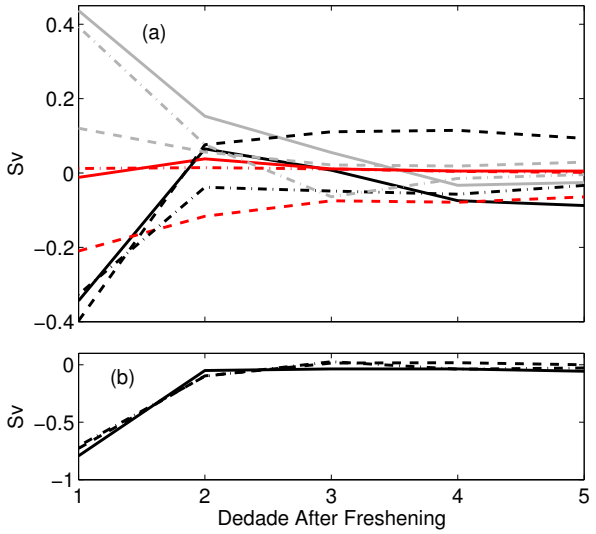

Figure 3. Anomalous freshwater flux into the northern North Atlantic (a) across ∼55°N on average (black lines), into the Arctic Ocean and Barents Sea (gray lines), and downward into the top surface in the region inbetween (red lines) and (b) the net flux (black plus red minus gray curves). (solid line = modern, dashed = LGM, dot-dash = $4XCO_2$). The transport is computed on the native model grid, which is not aligned with true latitudes and longitudes, so the transport across the southern boundary actually spans true latitudes from 53.2–58.6°N, depending on the longitude.

Auxiliary Reference

Gent, P. R, and G. Danabasoglu, Heat uptake and the thermohaline circulation in the Community Climate System Model, Version 2, *J. Clim.*, *17*, 4058–4069, 2004.